



Development and evaluation of processes affecting simulation of diel fine particulate matter variation in the GEOS-Chem model

Yanshun Li¹, Randall V. Martin^{1,2}, Chi Li¹, Brian L. Boys², Aaron van Donkelaar¹, Jun Meng³, Jeffrey R. Pierce⁴

¹Department of Energy, Environmental & Chemical Engineering, Washington University in St. Louis, St. Louis, Missouri, USA

²Department of Physics and Atmospheric Science, Dalhousie University, Halifax, Nova Scotia, Canada

³Air Quality Research Division, Environment and Climate Change Canada, Toronto, Ontario, Canada

⁴Department of Atmospheric Sciences, Colorado State University, Fort Collins, Colorado, USA

Correspondence to: Yanshun Li (yanshun.li@wustl.edu)

Abstract. The capability of chemical transport models to represent fine particulate matter (PM_{2.5}) over the course of a day is of vital importance for air quality simulation and assessment. In this work, we used the nested GEOS-Chem model at 0.25°×0.3125° resolution to simulate the diel (24 h) variation in PM_{2.5} mass concentrations over the United States (US) in 2016. We evaluate the simulations with in situ measurements from a national monitoring network. Our base case simulation broadly reproduces the observed morning peak, afternoon dip and evening peak of PM_{2.5}, matching the timings of these features within 1-3 hours. However, the simulated PM_{2.5} diel amplitude in our base case was 105% biased high relative to observations. We find that temporal resolution of emissions, differences in vertical representativeness between model and observations, as well as boundary layer mixing are the major causes for this inconsistency. We applied an hourly anthropogenic emission inventory and converted the PM_{2.5} masses from model level center to the height of surface measurements by correcting for aerodynamic resistance. The biases in the PM_{2.5} diel amplitude were reduced to 25% in the improved simulation and the timing of diel variations were better captured. In addition, notable sensitivity of the simulated diel amplitude of PM_{2.5} (8%) on the boundary layer height in the driving met fields were identified. Based on the improved model, we find that the diel variation in PM_{2.5} is driven by 1) building up of PM_{2.5} in early morning due to increasing anthropogenic emissions into a shallow mixed layer, 2) decreasing PM_{2.5} from mid-morning through afternoon associated with mixed layer growth, 3) increasing PM_{2.5} from mid-afternoon through evening as emissions persist into a collapsing mixed layer, and 4) decreasing PM_{2.5} overnight as emissions diminish.

1 Introduction

Airborne fine particulate matter (PM_{2.5}) affects human health (GBD 2019 Risk Factor Collaborators, 2020), visibility (Malm et al., 1994; Li et al., 2016) and the climate system (Pörtner et al., 2022). Accurately representing the diel PM_{2.5} variation, its variation over the course of a day, is essential for exposure assessment, air quality modeling and relating PM_{2.5} concentrations at a specific time of day to daily averages (van Donkelaar et al., 2010; Manning et al., 2018). Ground-level observations have revealed similar bimodal diel PM_{2.5} variations across the world, in which the mass



25 concentrations typically peak in morning and late evening, with minima near daybreak and late afternoon (Manning et al., 2018). How well chemical transport models (CTMs) reproduce this variation has not been fully investigated.

Previous modelling studies over major anthropogenic source regions found mixed levels of skill in resolving diel PM_{2.5} variation. CTMs generally well capture the observed mid-morning and late evening peaks in PM_{2.5} (Tessum et al., 2015; Bessagnet et al., 2016; Du et al., 2020). The peak in mid-morning is commonly attributed to enhanced anthropogenic emission activities and the peak in late evening ascribed to the collapse of planetary boundary layer (Zhao et al., 2009; Rattigan et al., 2010; Tiwari et al., 2013). Biases in simulated diel PM_{2.5} variation have also been identified and investigated. Du et al. (2020) found that over East Asia the WRF-Chem CTM (Grell et al., 2005) overpredicted nighttime PM_{2.5}, possibly due to insufficient boundary layer mixing. Simulations from multiple CTMs in the EURODELTA III intercomparison study (Bessagnet et al., 2016) found notable underestimation of PM_{2.5} in the afternoon over Europe. Lack of unspciated organics and incomplete chemical mechanisms for the formation of secondary organic aerosols were proposed as the driving forces.

40 The vertical extent of the first model level in CTMs is typically tens of meters above ground, while ground-based measurements are taken at around two meters. Therefore, vertical representativeness differences exist between CTMs and ground-based observations, which can affect model evaluation. Previous modeling studies have estimated subgrid vertical gradients in HNO₃ and O₃ within the first model level using dry deposition velocity and aerodynamic resistance (Zhang et al., 2012; Travis and Jacob, 2019). How such differences in vertical representation affect simulated diel PM_{2.5} has not been investigated. Aerosol dry deposition, defined as the removal of pollutants by gravitational settling, Brownian diffusion, or by impaction and interception resulting from turbulent transfer (Beckett et al., 1998), is an important sink process which may also affect the diel variation of PM_{2.5}.

45 In this work, we use the GEOS-Chem CTM, initially described by Bey et al. (2001), to investigate the diel variation in simulated PM_{2.5}. We focus on the US in 2016. In Sect. 2, we introduce the GEOS-Chem model and the configurations of our base simulation. In Sect. 3, we describe the in situ measurements of PM_{2.5}. The rest of the paper is organized by themes, each of which contain its own methodology, results and discussions. In Sect. 4, we evaluate and identify biases of the simulated diel PM_{2.5} variation by our base GEOS-Chem simulation. Multiple physical and chemical processes affecting the diel PM_{2.5} simulation are explored in Sect. 5 by developing the model and conducting sensitivity simulations, based on which we describe the revised diel simulation with discussions in Sect. 6. Sect. 7 concludes this study.

2 The GEOS-Chem model and the base simulation

2.1 General description

55 We use the GEOS-Chem model version 12.6.0 (www.geos-chem.org) to examine the factors controlling the diel PM_{2.5} mass variations. GEOS-Chem is a three-dimensional chemical transport model driven by assimilated meteorology from the NASA Global Modeling and Assimilation Office (GMAO). Applications of the model on PM_{2.5} studies include but are not limited to evaluating and improving mechanisms for PM_{2.5} formation (Zheng et al., 2015; Marais



60 et al., 2016; Song et al., 2021), source attribution (Meng et al., 2019; McDuffie et al., 2021; Pai et al., 2022), assessments of the effects of horizontal transport on local air quality (Lang et al., 2012; H. Zhang et al., 2019; Xu et al., 2023) and exposure assessments (Kodros et al., 2016; van Donkelaar et al., 2021).

65 GEOS-Chem simulates detailed tropospheric aerosol-oxidant chemistry which includes the sulfate-nitrate-ammonium system (Park et al., 2004; Fontoukis and Nenes, 2007), black carbon (Wang et al., 2014), organic carbon, secondary organic aerosol (Pai et al., 2020), mineral dust (Fairlie et al., 2007) and seasalt (Jaeglé et al., 2011). Absorption of radiation by brown carbon is implemented following Hammer et al., (2016). We use nested simulations over the US in 2016 at $0.25^\circ \times 0.3125^\circ$ over 47 vertical layers extending from surface up to 0.1 hPa. The surface level extends from ground to about 120 meters. The GEOS-5 Forward Processing (GEOS-FP) product from GMAO is used as the meteorological inputs, which includes hourly surface variables and 3-D variables at every 3 hours. A global simulation at $2^\circ \times 2.5^\circ$ is used to provide the boundary conditions for the nested domain. The non-local scheme implemented by Lin and McElroy (2010) is used for boundary layer mixing.

70 In this work, we start from evaluating the base simulation of GEOS-Chem (see GC_Base in Table 1). We identify the biases of diel $PM_{2.5}$ in the base simulation by comparing with in situ observations. Then by developing different model components and conducting sensitivity simulations, we explore the driving forces of diel $PM_{2.5}$ and improve the simulation. Sect. 2.2 and 2.3 will introduce the emission configuration and default parameterization of dry deposition in GC_Base.

75 **Table 1. Summary of modifications made to base GEOS-Chem simulation to investigate diel $PM_{2.5}$ variation.**

GEOS-Chem simulation	Emission Inventory	Vertical gradient resolved	Dry deposition revised	Adjustments on PBLH
GC_Base	NEI monthly	No	No	No
GC_Emis	NEI hourly	No	No	No
GC_Drydep	NEI hourly	No	Yes	No
GC_2m	NEI hourly	Yes	Yes	No
GC_2m_PBLH	NEI hourly	Yes	Yes	Yes

2.2 Emissions configurations in GC_Base

80 To investigate the impacts of anthropogenic emissions, we use the monthly version of the National Emission Inventory (NEI) in GC_Base instead of the default hourly version in the standard nested GEOS-Chem model over North America, which is consistent with most regions out of the US where anthropogenic emissions at hourly resolution are often not readily available. The base year of NEI is 2011. We scale the NEI emissions to 2016 by using the air pollutant emissions trend data provided by the US Environmental Protection Agency (EPA) (<https://www.epa.gov/air-emissions-inventories/air-pollutant-emissions-trends-data>). Point sources in the NEI inventory mainly include large industrial facilities, power plants and airports. Nonpoint sources mainly include residential heating, transportation,



85 commercial combustion and solvent use. For wildfires, we use GFED4 (Giglio et al., 2013) 3-hourly emissions. For dust, we use the hourly offline inventory developed by Meng et al. (2021).

2.3 Dry deposition parameterization in GC_Base

Dry deposition of $PM_{2.5}$ in our base GEOS-Chem simulation generally follows the Zhang et al. (2001) scheme (henceforth Z01), which parameterizes particle dry deposition velocities (V_d) by accounting for gravitational settling (V_g), aerodynamic resistance (R_a) and surface resistance (R_s), as shown in Eq. (1):

$$90 \quad V_d = V_g + \frac{1}{R_a + R_s}, \quad (1)$$

Gravitational settling represents the particle settling due to gravity. Aerodynamic resistance describes the turbulent transport of scalars within the surface layer. Surface resistance, as formulated in Eq. (2), quantifies particle-surface contact in close proximity to surfaces by Brownian diffusion (E_b), impaction (E_{Im}) and interception (E_{Int}).

$$R_s = \frac{1}{\varepsilon_0 u_* (E_b + E_{Im} + E_{Int}) R_1}, \quad (2)$$

95 where u_* denotes friction velocity, R_1 denotes a bounce correction term and ε_0 denotes an empirical coefficient. Brownian diffusion contributes to dry deposition through diffusion when particles are close to surface collectors. Impaction describes the direct collision of particles to surfaces due to inertia when particles move along the streamlines around collector surfaces. Interception represents the deposition by which particles are captured by surface collectors when their distances to the collectors are less than the radius of a single particle.

100 The standard GEOS-Chem dry deposition module used in our base simulation calculates dry deposition velocity (V'_d) following Eq. (3), where gravitational settling is ignored.

$$V'_d = \frac{1}{R_a + R_s}, \quad (3)$$

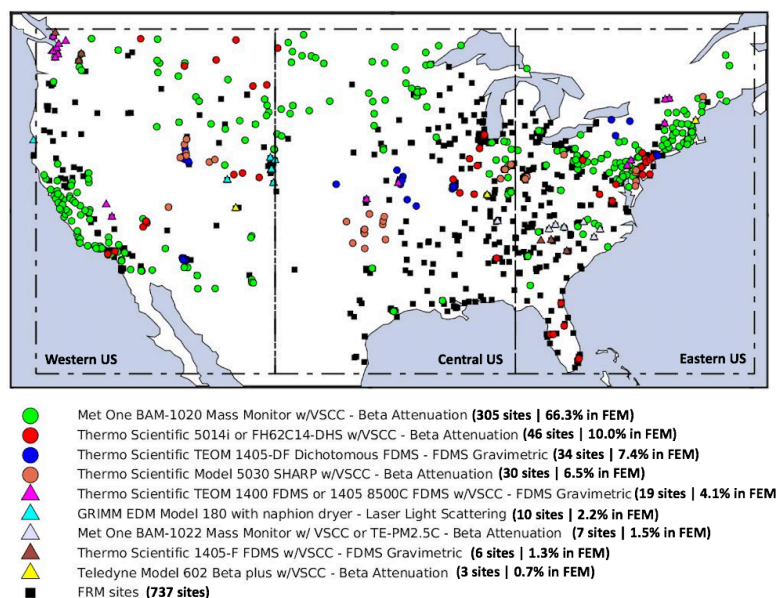
105 The dry deposition of $PM_{2.5}$, including sulfate, nitrate, ammonium, organics, black carbon, fine mode seasalt and fine mode mineral dust components are calculated. Information about particle size is important, as all terms in Eq. (1-3) are size-dependent except aerodynamic resistance R_a . The dry deposition module in the base GEOS-Chem simulation has inconsistencies with other modules that we address in Sect. 5.2. In the standard GEOS-Chem dry deposition module, fine mode mineral dust is considered in two size bins with mass-weighted mean diameters of 1.46 and 2.80 μm . Other components are each considered in a single size bin with mass-weighted mean dry diameters for sulfate, nitrate, ammonium, organics, black carbon and fine mode seasalt of 0.5 μm . Monodisperse size distributions are used
110 for all size bins. The effect of hygroscopic growth on deposition is only considered for fine mode seasalt following Lewis and Schwartz (2006). We use the standard GEOS-Chem dry deposition module for our base simulation.

3 In situ measurements of $PM_{2.5}$

The in situ measurements from the United States Environmental Protection Agency's Air Quality System (AQS) are used to evaluate the GEOS-Chem simulations. There were 451 sites operating in 2016 across the US which provided



115 hourly PM_{2.5} concentrations using a Federal Equivalency Method (FEM). As depicted in Fig. 1, 66.3% of these FEM
 sites equipped with the Met One BAM-1020 Mass Monitor using Beta Attenuation, 10.0% equipped with the Thermo
 Scientific 5014i/FH62C14-DHS Monitor using Beta Attenuation, 7.4% equipped with the Thermo Scientific TEOM
 1405-DF Dichotomous Monitor using FDMS Gravimetric and 6.5% equipped with the Thermo Scientific 5030
 SHARP Monitor using Beta Attenuation. These four types of FEM monitors are used for hourly analysis in this work.
 120 The other five types of FEM instruments, contributing less than 10% of all hourly measurements, are excluded to
 avoid risk of aliasing instrument-dependent and regionally dependent characteristics. Further detail about
 instrumentation is provided in supplemental Sect. S1. A small fraction (0.05%) of the FEM measurements exceeding
 ten times their standard deviation are suspicious of strong fire contamination and present significant modulation on
 the regional diel variation pattern and are excluded as outliers from the focus of this study. Also shown in Fig. 1 are
 125 the additional 737 sites using Federal Reference Method (FRM) to measure 24-hour average PM_{2.5} concentrations
 which significantly improve observational coverage of the US for the evaluation of spatial distribution of GEOS-
 Chem simulated PM_{2.5}.



130 **Figure 1. Spatial distribution of the US EPA PM_{2.5} measurements. Colored markers represent Federal Equivalency Method (FEM) sites equipped with different kinds of instruments which report hourly PM_{2.5} concentrations. Black squares represent Federal Reference Method (FRM) sites which report 24-hour average PM_{2.5}.**

4 Diel PM_{2.5} variation in the base GEOS-Chem simulation and the FEM measurements

We first examine the diel PM_{2.5} variation in the base simulation. Fig. 2a shows annual-mean diel PM_{2.5} variation across the US from the FEM in situ observations and the space and time co-located base GEOS-Chem simulation. The



135 observed $PM_{2.5}$ shows a typical diel cycle consistent with previous work (Manning et al., 2018). The concentrations
 peak at mid-morning, diminish until late afternoon, increase in evening and remain elevated throughout the night. The
 base GEOS-Chem simulation broadly captures these features with their timings accurate within 1-3 hours. The
 simulated concentration decreases from morning to late afternoon then increases throughout the evening, consistent
 with the diel cycle of growth and collapse of the boundary layer. However, the simulated $PM_{2.5}$ is significantly
 140 overestimated at night, especially from midnight to early morning when the GEOS-Chem $PM_{2.5}$ increases beyond the
 standard deviation of the observations during which time the observations exhibit a slight decrease. The nighttime
 model overestimation leads to a 105% positive bias in the $PM_{2.5}$ diel amplitude, defined as the difference between the
 maximum and the minimum of the normalized diel concentration. The Root Mean Square Deviation (RMSD) of
 annual diel variation in $PM_{2.5}$ between the base simulation and the observations is $3.26 \mu\text{g}/\text{m}^3$. The spatial distribution
 145 of $PM_{2.5}$ in the base GEOS-Chem simulation is discussed in supplemental Sect. S2.

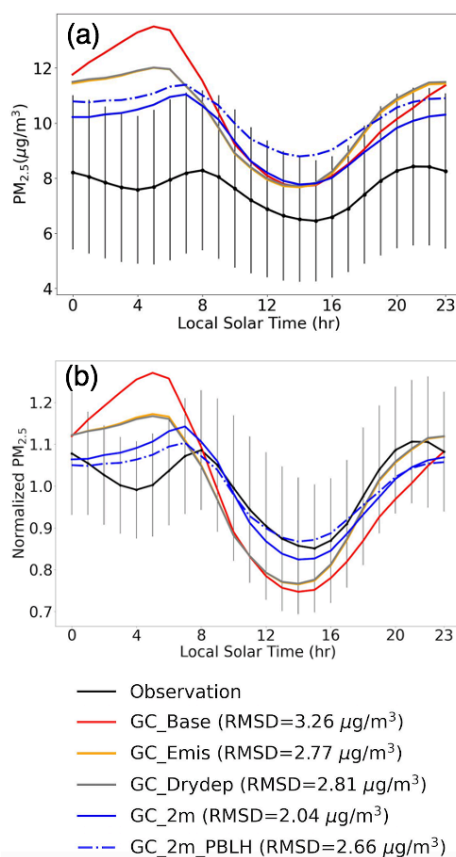


Figure 2. (a) Annual mean diel $PM_{2.5}$ variation over the US in 2016. (b) Normalized annual mean diel $PM_{2.5}$ from GEOS-Chem (GC) sensitivity simulations over the US in 2016. Vertical lines indicate the spatial standard deviations of annual-mean $PM_{2.5}$ for the FEM measurements at each hour.



150 5 Development of processes affecting simulation of diel PM_{2.5}

We develop and evaluate the processes affecting the simulation of diel PM_{2.5} variation in GEOS-Chem with particular attention to the driving forces of the nighttime bias. We focus on the temporal resolution of emissions, aerosol dry deposition, vertical representativeness, boundary layer mixing and dew formation, as summarized in Table 1.

5.1 Impacts from the temporal resolution of emissions

155 We examine the temporal resolution of anthropogenic emissions as the first source of the nighttime PM_{2.5} positive bias identified in Sect. 4. Fig. 3 shows the normalized mean diel emission profile for different species in the hourly version of the NEI inventory. Anthropogenic emissions are notably higher during the day than at night, with minima from midnight to early morning in the emission intensities for every primary species. The diel amplitude of SO₂ emissions is the weakest, driven by persistent power plant emissions. NH₃ emissions have the strongest diel amplitude, driven by a temperature dependence for this predominantly agriculturally emitted species over the US (Zhang et al., 2018).
160 Fig. S3 in the supplemental depicts the normalized mean emission strengths for species in Fig. 3 both seasonally and regionally. The early afternoon NH₃ peak depicted in Fig. 3 is found most prominent over summertime Central US in Fig. S3, in accordance with the temperature-dependant agricultural emissions of NH₃. Primary emissions of particulate organic carbon (OC) have a peak near 18:00 LT (Local Time), corresponding to more intense residential heating. The
165 OC emissions in evening are strongest during winter as shown in Fig. S3, reflecting the seasonality of residential combustion activities (Li and Martin, 2018).

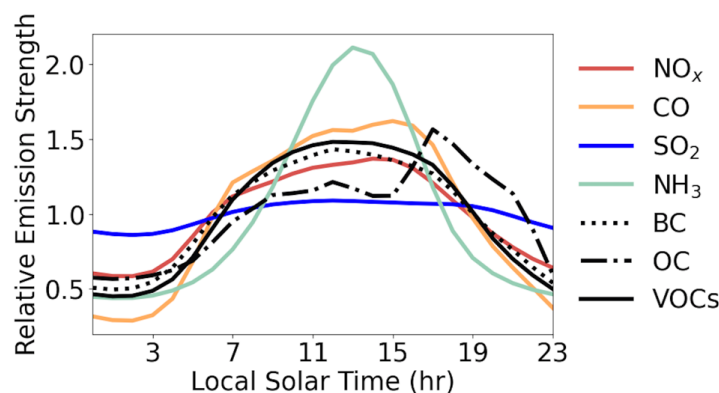


Figure 3. Normalized mean diel emission profile for different species across the US.

To evaluate the impacts from the temporal resolution of emissions, we conduct a sensitivity simulation GC_Emis (Table 1) which replaces the monthly NEI in GC_Base with the hourly NEI. Fig. 2b shows that GC_Emis simulates a much weaker PM_{2.5} accumulation from midnight to early morning relative to GC_Base, mainly due to the lower emission intensities of aerosol sources throughout the night in the NEI hourly inventory. In the evening, PM_{2.5} in the GC_Emis simulation accumulates slightly faster than the base case, reflecting the stronger precursor emissions in daytime after applying the hourly inventory. The RMSD between GC_Emis diel PM_{2.5} and the FEM observations



175 decrease from $3.26 \mu\text{g}/\text{m}^3$ in GC_Base to $2.77 \mu\text{g}/\text{m}^3$, and the positive bias in the diel amplitude drops from 105% to 60%. Overall, the temporal resolution of emissions explains 43% of the modeling bias in diel amplitude. Daytime $\text{PM}_{2.5}$ is insensitive to changes in diel emission profiles. During the night, the impacts of emissions on $\text{PM}_{2.5}$ levels are more prominent, especially from midnight to early morning when the boundary layer is more stable. From this perspective, the slight overnight reduction of $\text{PM}_{2.5}$ in the FEM measurements is likely driven by the sharp decline in anthropogenic emissions. Nevertheless, the diel emission profile does not fully explain the diel biases identified in Sect. 4. Other contributing factors exist.

5.2 Impacts from the dry deposition parameterizations

We explore dry deposition as the second potential source for the diel-varying biases in the base GEOS-Chem simulation. First, as described in Sect. 2.3, the dry deposition scheme in the base GEOS-Chem model does not account for gravitational settling V_g , which leads to systematic underestimation in particle dry deposition velocities. To improve on this missing consideration, we strictly follow Eq. (1) of Zhang et al. (2001), updating the gravitational settling term V_g to be explicitly considered when deriving the deposition velocity (Eq. 1). Second, the parameterization of surface resistances (Eq. 2) in the base scheme was developed when few particle deposition measurements were available. Following recent observational evidence, Emerson et al. (2020) identified that the Brownian diffusion E_b in Z01, as used in the standard GEOS-Chem model, is excessive while the contribution from interception E_{In} is too weak. We update the surface resistances R_s in GEOS-Chem by applying observationally-constrained Brownian diffusion E_b , impaction E_{Im} and interception E_{In} terms following observational evidence in Emerson et al. (2020). Formulations of E_b , E_{Im} , and E_{In} are updated following Table 2.

Table 2. Formulations for particulate gravitational setting (V_g), Brownian diffusion (E_B), interception (E_{IN}) and impaction (E_{IM}) used in the calculation of deposition velocity (V_d).

Resistance Model	V_g	E_B	E_{IN}	E_{IM}
Vd_Base	-	$Sc^{-\gamma}$	$\frac{1}{2} \left(\frac{D_p}{A}\right)^2$	$\left(\frac{St}{\alpha + St}\right)^2$
Vd_Z01	$V_g = \frac{\rho D_p^2 g C}{18\eta}$	$Sc^{-\gamma}$	$\frac{1}{2} \left(\frac{D_p}{A}\right)^2$	$\left(\frac{St}{\alpha + St}\right)^2$
Vd_Revised	$V_g = \frac{\rho D_p^2 g C}{18\eta}$	$0.2Sc^{-2/3}$	$\frac{5}{2} \left(\frac{D_p}{A}\right)^{0.8}$	$\frac{2}{5} \left(\frac{St}{\alpha + St}\right)^{1.7}$

A: characteristic radius for interception in Zhang et al. (2001).

C: the Cunningham correction factor.

D_p : Particle diameter.

g : gravitational acceleration constant

200 Sc : the Schmidt number.

St : the Stokes number.

V_g : gravitational settling velocity.



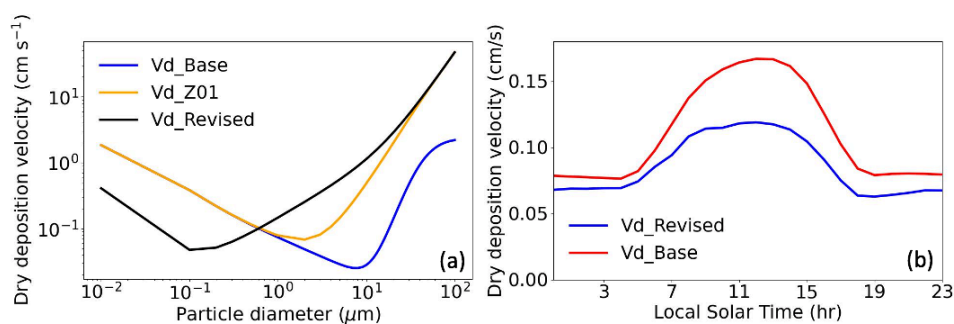
α : LUC-specific constant used in the impaction efficiency in Zhang et al. (2001), where LUC represents land use classification.

γ : LUC-specific exponent used in the Brownian diffusion efficiency in Zhang et al. (2001), which ranges from 0.5 to 0.58.

205 ρ : density of particle

η : viscosity of air

Fig. 4a shows V_g as a function of particle diameter for the base (Vd_Base) and revised (Vd_Revised) parameterizations, as well as according to the Z01 scheme (Vd_Z01). As seen in comparing Vd_Base and Vd_Z01 curves, inclusion of V_g in the calculation of V_d for the Vd_Z01 case substantially increases dry deposition velocities for particles larger than 2 μm in diameter. The Vd_Revised curve in the figure shows that implementing observational constraints on the surface resistances shifts the minimum in V_d to a particle diameter of around 0.1 μm , reflecting a weakened Brownian diffusion term and an enhanced interception term. It was shown by Emerson et al. (2020) that the parameterized size dependent particle dry deposition velocities are more consistent with observations after implementing these observational constraints. To further evaluate the impact of particle V_d on diel PM_{2.5}, the representation of aerosol size distributions in the dry deposition scheme of GEOS-Chem, including hygroscopic growth, must be considered.



220 **Figure 4. (a) Size-resolved particle dry deposition velocities over grassland land type from GEOS-Chem. (b) Diel mean dry deposition velocities for sulfate aerosol over the US in 2016. Vd_Base represents the default dry deposition scheme in the base GEOS-Chem model (Eq. 3). Vd_Z01 includes the effect of gravitational settling on Vd_Base (Eq. 1). Vd_Revised further implements the observational constraints on the surface resistance terms, as discussed in Sect. 5.2.**

As introduced in Sect. 2.3, the dry deposition scheme in the standard GEOS-Chem model assigns a single unreferenced mass-weighted mean diameter to different PM_{2.5} components. We update the mass-weighted mean diameter for each aerosol species dry deposited to be consistent with the sizes in the GEOS-Chem radiation module. We implicitly consider aerosol size distributions based on mass conservation principles:

225
$$\int_0^\infty n(D_p) \cdot \frac{4}{3}\pi \left(\frac{D_p}{2}\right)^3 \cdot \rho \cdot V_d(D_p) dD_p = N \cdot V_d(D_p^*) \cdot \frac{4}{3}\pi \left(\frac{D_p^*}{2}\right)^3 \cdot \rho, \quad (4)$$

where D_p denotes particle diameter, $n(D_p)$ represents the particle number size distribution, ρ denotes the particle density, $V_d(D_p)$ denotes the size-dependent particle dry deposition velocity, N denotes the total particle number



concentration integrated across the aerosol size distribution, D_p^* denotes the mass-weighted mean dry diameter for a specific aerosol species and $V_d(D_p^*)$ denotes the dry deposition velocity of a particle with diameter of D_p^* . The size distribution for each $PM_{2.5}$ component was acquired from Latimer and Martin (2019). The updated mass-weighted mean dry diameter for sulfate, nitrate, ammonium and organic aerosols is $0.17 \mu\text{m}$, for fine mode seasalt is $0.23 \mu\text{m}$, and for the fine mode mineral dust in two size bins are $0.67 \mu\text{m}$ and $2.49 \mu\text{m}$.

The standard GEOS-Chem dry deposition module only considers the hygroscopic growth of fine mode seasalt. Omitting hygroscopicity for other $PM_{2.5}$ components may lead to biases in the simulated dry deposition velocities and thus affect the diel variation of $PM_{2.5}$. Here we implement hygroscopic growth in the dry deposition parameterization for sulfate, nitrate, ammonium (SIA) and organic components (OA) of $PM_{2.5}$ by application of a κ -Kohler growth function to the mass-weighted mean dry diameters (Petters and Kreidenwei 2007, 2008, 2013; Latimer and Martin, 2019). Fine mode dust and black carbon are treated as hydrophobic. The κ -Kohler growth factor is calculated as:

$$GF = \left(1 + \kappa \frac{RH}{100 - RH}\right), \quad (5)$$

The hygroscopicity parameters κ for SIA are set as 0.61 and for OA are set as 0.1 respectively (Latimer and Martin, 2019). Efflorescence transitions are considered for the SIA components (Latimer and Martin, 2019). For fine mode seasalt, we continue to use the growth function from Lewis and Schwartz (2006).

Taking the sulfate component in $PM_{2.5}$ as an example, Fig. 4b presents the combined impacts of all the updates above on the diel dry deposition velocities. Implementation of gravitational settling and hygroscopic growth tends to increase the sulfate dry deposition velocity, compensating for the lower revised aerosol dry deposition velocities, mainly due to the revised scheme using a smaller mass-weighted mean dry diameter. The reductions of deposition velocity in the revised case are more prominent during daytime, when the size-dependent surface resistances dominate the dry deposition processes. In the revised profile, from midnight to early morning (0am-6am), the dry deposition velocities are 10.4% higher than those in the evening (18pm-0am), reflecting the stronger aerosol hygroscopic growth due to higher relative humidity. We evaluate the impacts on simulated diel $PM_{2.5}$ masses in GEOS-Chem as GC_Drydep simulation (Table 1) which adds all the deposition updates to GC_Emis. Fig. 2b shows that the diel $PM_{2.5}$ masses simulated by GC_Drydep and GC_Emis are almost identical. The insensitivity of diel variation of $PM_{2.5}$ to dry deposition updates implies that the diel $PM_{2.5}$ biases identified in Sect. 4 are unlikely to be caused by the uncertainty of the GEOS-Chem dry deposition module.

5.3 Impacts from the vertical representativeness differences between model and observations

The third possible contributor to the $PM_{2.5}$ nighttime biases that we consider is the vertical representativeness difference between model and observations. Given the vertical extent of the lowest model level (120 m), simulated concentrations represent an average over a greater depth than the FEM measurements typically taken at around 2 meters. This difference in vertical representation may be especially problematic for model-measurement comparison during periods of diabatic stability resulting in strong near-surface concentration gradients. Vertical concentration gradients within 120 m of the surface have been widely observed for aerosol species in previous field campaigns.



265 Sievering et al. (1994) measured the vertical profiles of aerosols over the Bayerischer Wald National Park in Germany using filter pack sampling, reporting 2 m concentrations lower than at 51 m for nitrate (51%), ammonium (81%) and sulfate (81%). In the Utah Winter Fine Particulate Study, the PM_{2.5} concentrations measured by three ground sites at Logan, Cache, Salt Lake Valley and the Utah Valley were around 70% of those at around 50 meters measured by aircraft (Franchin et al., 2018). Thus, the PM_{2.5} simulated by GEOS-Chem is intrinsically different from the FEM in situ measurements because of the mismatch of vertical sampling location.

270 To evaluate the impact of these vertical representativeness differences, we developed the GC_2m simulation (Table 1), in which PM_{2.5} from the lowest model level of the GC_Drydep simulation is adjusted to the height of the FEM measurements (2 meters above ground). The conversion process quantifies the vertical concentration gradient of secondary PM_{2.5} components by using the resistance-in-series formulation for dry deposition following previous studies (Zhang et al., 2012; Travis and Jacob, 2019). The mathematical formula is described in Eq. 6,

$$C(z_{2M}) = [1 - R_a(z_{2M}, z_{GBC})V_d(z_{GBC})]C(z_{GBC}), \quad (6)$$

275 where $C(z_{2M})$ and $C(z_{GBC})$ represent the concentrations at measurement height of 2 meters and the grid-box-center of the GEOS-Chem surface layer (around 60 meters) respectively, $R_a(z_{2M}, z_{GBC})$ represents the aerodynamic resistances between the measurement height and the grid-box-center, $V_d(z_{GBC})$ represents the dry deposition velocity. $R_a(z_{2M}, z_{GBC})$ is calculated using the Monin-Obukhov similarity theory:

$$R_a(z_{2M}, z_{GBC}) = \int_{z_{GBC}}^{z_{2M}} \frac{\Phi(\zeta)}{ku^*\zeta} d\zeta, \quad (7)$$

280 where $\zeta = z/L$. L denotes the Monin-Obukhov length which is determined by surface momentum fluxes and sensible heat. Φ represents a function of stability described by Businger et al. (1971). k represents the von Karman constant and u^* represents the friction velocity. The method requires a boundary condition of zero concentration at ground. Thus, it is only applied to secondary PM_{2.5} components, not primary components with surface emission fluxes.

285 Fig. 2b shows the normalized annual curves of GC_2m across the US. Comparison of GC-Drydep and GC_2m indicates that the vertical correction effectively suppresses the excessive PM_{2.5} levels from midnight to early morning and sustains the daytime concentration variation due to boundary layer mixing. The bias of diel amplitude of the corrected GC_2m PM_{2.5} is reduced to 25% against the FEM observations. In terms of absolute concentrations, the average reduction from GC_Drydep to GC_2m is 1.20 $\mu\text{g}/\text{m}^3$ during 6pm-6am (nighttime), while that for 6am-6pm (daytime) is 0.12 $\mu\text{g}/\text{m}^3$. This day-night contrast is consistent with a previous DISCOVER-AQ field study (Prabhakar et al., 2017), in which the vertical gradient of nitrate aerosols measured by aircraft was significantly greater in a stable surface layer than in a turbulent surface layer. At night, under a stable boundary layer, surface resistances are suppressed due to weaker particle impaction and interception. Aerodynamic resistances then become relatively stronger with the resulting correction in Eq. 6 yielding a greater reduction of PM_{2.5} concentrations. During the day, as boundary layer mixing strengthens, surface resistances dominate over the aerodynamic resistances and the correction in Eq. 6 is weaker. Resolving the vertical representativeness differences enables the GEOS-Chem simulation to better capture the timings of the observed overall PM_{2.5} morning peak and afternoon minimum across the US. In the GC_Drydep simulation, the PM_{2.5} morning peak and afternoon minimum are three hours and one hour earlier than the

295



FEM observations respectively. After the vertical correction, in the GC_2m simulation, the morning peak appears only one hour ahead of the observations, and the timing of the afternoon minimum matches the observations without bias.

300 5.4 Impacts from boundary layer height

Planetary boundary layer height (PBLH) is investigated as the next possible source of the biases identified in Sect. 4. PBLH is closely related to boundary layer mixing, which significantly affects diel PM_{2.5} (Du et al., 2020). Uncertainties exist in PBLH datasets estimated from different meteorological sources and using different algorithms. In this section, to investigate the sensitivity of simulated diel PM_{2.5} in GEOS-Chem on PBLH, we adjust the GEOS-FP planetary boundary layer height (PBLH) which used for driving GEOS-Chem by using the PBLH derived from the Aircraft Meteorological Data Reports (AMDAR) at 54 sites (Fig. S4) across the US (Zhang et al., 2020) as reference.

Fig. 5 shows the seasonal variation in PBLH. The observed PBLH from AMDAR shows similar diel variation across all seasons, which stays low from midnight to early morning, increases to a maximum in mid-afternoon, then decreases throughout rest of the day. In terms of absolute amplitude, the AMDAR PBLH are higher during spring and summer, mainly due to strong near-surface wind speed and intense solar radiation (Guo et al., 2016). The GEOS-FP reanalysis generally captures the diel variation of the AMDAR PBLH over all seasons, albeit with overestimates during daytime (7:00-19:00 LT), which is consistent as previous comparison studies (Millet et al., 2015; Zhu et al., 2016). The GEOS-FP PBLH is highest in summer and lowest in winter, which is inconsistent with the AMDAR PBLH maximum in spring.

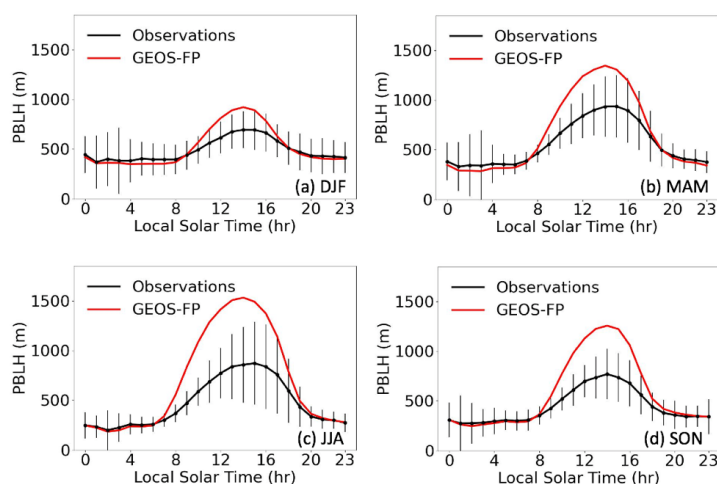


Figure 5. Seasonal diel variation of AMDAR (observation-based) and GEOS-FP PBLH. Vertical bars indicate the spatial standard deviations of AMDAR PBLH.



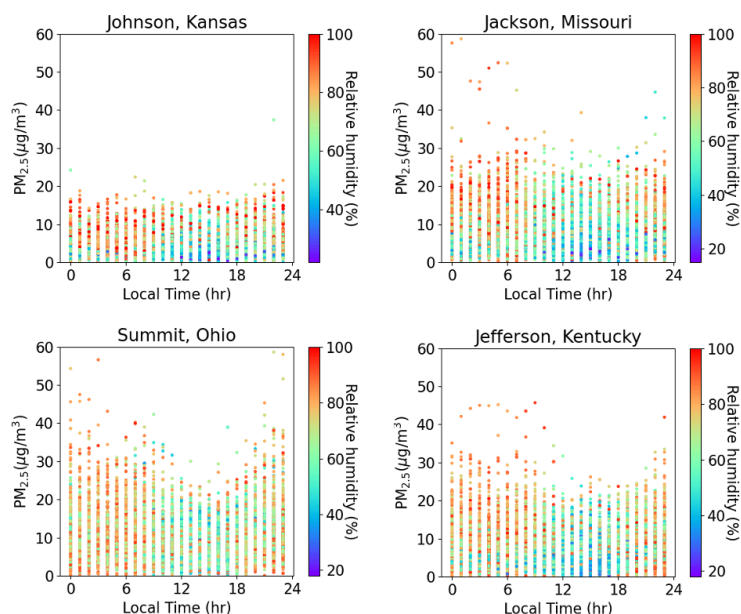
320 To quantify the impacts of the uncertainty in PBLH on modeled diel $PM_{2.5}$, we develop the GC_2m_PBLH simulation
(Table 1) in which the GEOS-FP PBLH used in the GC_2m simulation is adjusted by the AMDAR observations.
Specifically, we matched the hourly AMDAR and GEOS-FP PBLH over the US spatially and temporally, then derived
US-averaged (0-23 h) adjustment factors for different seasons following Eq. 8:

$$AF_{i,j} = \frac{\overline{PBLH_{AMDAR_{i,j}}}}{\overline{PBLH_{GEOS-FP_{i,j}}}}, \quad (8)$$

325 where $AF_{i,j}$ represents the PBLH adjustment factor for season i and hour j , $\overline{PBLH_{AMDAR_{i,j}}}$ represents the US-averaged
AMDAR PBLH for season i and hour j , and $\overline{PBLH_{GEOS-FP_{i,j}}}$ represents the US-averaged GEOS-FP PBLH for season
 i , hour j . Implementing this adjustment scales the GEOS-FP PBLH to the same seasonal diel value as the AMDAR
PBLH over the US. Applying these adjustment factors to the GEOS-FP PBLH, as shown in blue and dashed in Fig.
2b, reduces the biases in simulated $PM_{2.5}$ diel amplitude against the FEM observations by 8%. Owing to the sparsity
of the AMDAR network and uncertainties in both PBLH sources, we only emphasize the importance of boundary
330 layer height in simulating diel $PM_{2.5}$ mass variations in GEOS-Chem, without including the PBLH adjustment in the
final revised simulation.

5.5 Impacts from dew formation

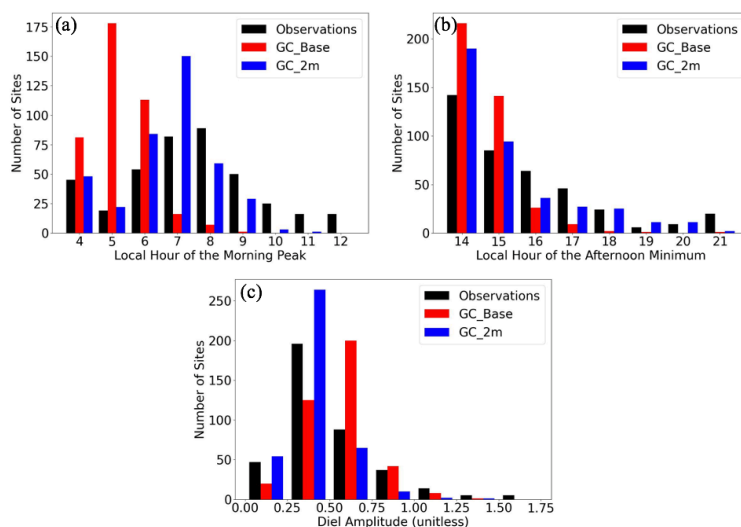
We also examined the possibility of dew formation as a potential process affecting the diel variation in $PM_{2.5}$. It was
reported that the condensation process during the formation of dew involves removal of airborne particles from the
335 atmosphere (Polkowska et al., 2008; Muskała et al., 2015). We considered whether the observed $PM_{2.5}$ decrease from
midnight to early morning (Fig. 2) might be partly ascribed to this mechanism, and thus contribute to the overestimated
nighttime $PM_{2.5}$. However, based on two lines of reasoning, we conclude here that dew formation is unlikely to
significantly affect the diel $PM_{2.5}$ mass variations over the US. First, we examined co-located hourly RH and $PM_{2.5}$
mass concentrations at 37 sites in 2016 across the US. Fig. 6 shows four examples. We found no evidence of
340 correlation of low $PM_{2.5}$ masses and high nighttime RH values ($r=0.16/0.18/0.13/0.15$ for Johnson, Kansas/Jackson,
Missouri/Summit, Ohio/Jefferson, Kentucky). Second, the decreases of $PM_{2.5}$ overnight are found sharpest in the
Western US where the average relative humidity (RH) is lowest among all subregions, which indicates that dew
formation at high RH condition is unlikely an important driving factor.



345 **Figure 6. Co-located relative humidity (RH) and $PM_{2.5}$ mass concentrations at four example sites. Each point represents the measured hourly $PM_{2.5}$ concentration at the measured hourly RH for each site. The RH measurements are provided by the NOAA Local Climatological Data (LCD) program. The $PM_{2.5}$ mass concentrations are provided by the EPA FEM sites.**

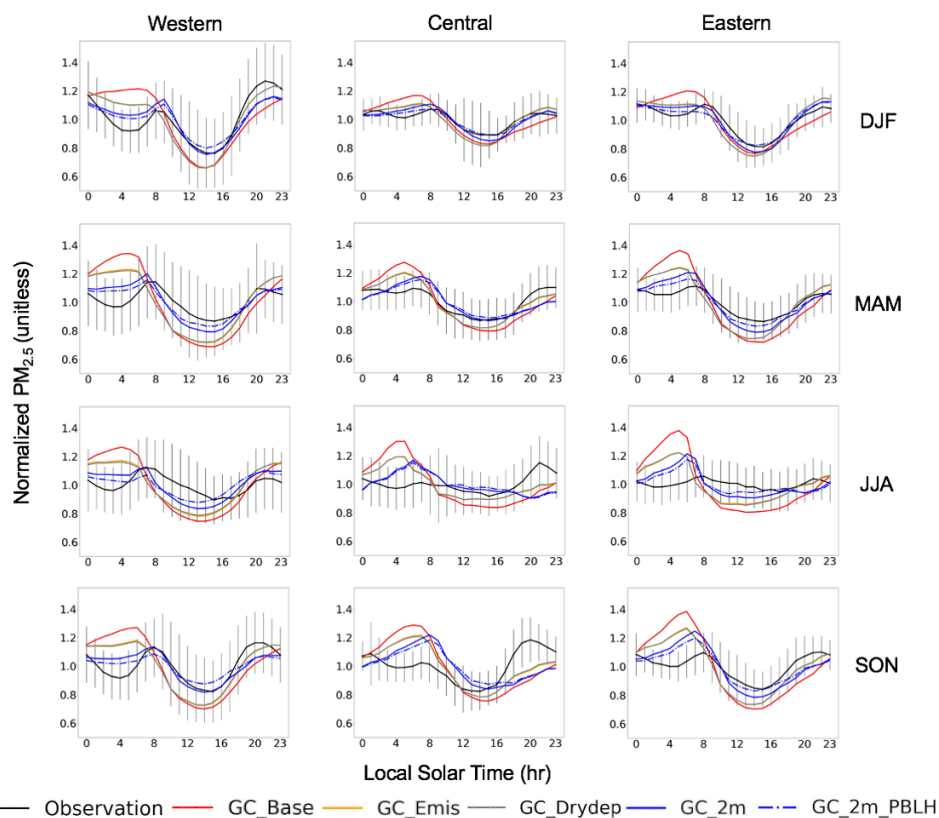
6 Discussion of diel $PM_{2.5}$ variation in the final revised GEOS-Chem simulation (GC_2m)

350 Overall updating the temporal resolution of emissions, dry deposition parameterizations and resolving the vertical representative differences between model and observations notably improves the diel variation of $PM_{2.5}$ in GC_2m relative to GC_Base. In the annual diel comparison averaged across the US (Fig. 2), the bias in the $PM_{2.5}$ diel amplitude in GC_2m (25%) is significantly reduced relative to GC_Base (105%). The average observed $PM_{2.5}$ morning peak and afternoon minimum are at 8:00 LT and 15:00 LT respectively. GC_Base simulates them with biases of -3 and -1
355 hours while GC_2m reduces these to -1 and 0 hours. In addition to the average comparison across the country, we further explore the performances over all FEM sites. Fig. 7 shows histograms of the timing of the morning peak, of the afternoon minimum, and of the diel amplitude. At most FEM sites, GC_Base tends to overestimate the $PM_{2.5}$ diel amplitude and simulates the $PM_{2.5}$ diel features too early. By correcting for the vertical representativeness differences and using emissions with hourly temporal resolution, these biases are largely addressed in GC_2m with the distribution
360 in the histogram better matching observations. The RMSD of diel $PM_{2.5}$ between GC_2m and the FEM observations decreases from 3.26 to 2.04 $\mu\text{g}/\text{m}^3$. By reducing the 24-hour averaged $PM_{2.5}$ concentration, GC_2m also improves the comparison of annual-mean $PM_{2.5}$ against the FEM/FRM measurements across the US (supplemental Sect. 2).



365 **Figure 7. Distribution of simulated and observed PM_{2.5} features over the FEM sites. (a) Timing of morning peak. (b) Timing of afternoon minimum. (c) Diel Amplitude.**

370 Fig. 8 shows the diel variation of PM_{2.5} in different seasons and subregions. The observed diel PM_{2.5} variations are generally similar to the annual results across the country, suggesting consistent mechanisms controlling the local cycles. The observed PM_{2.5} diel amplitude is smallest during summer, as the observed concentrations decrease more slowly from mid-morning to late afternoon than in other seasons. The GC_2m simulation generally reproduces this summer minimum in diel amplitude, improving on GC_Base which simulates the minimum amplitude in winter, by reducing excess PM_{2.5} at night, by reducing PM_{2.5} precursor emissions and by accounting for vertical representativeness differences at night. Stronger photochemical production of PM_{2.5} during daytime in summer than other seasons, also counteracts the ventilation by boundary layer mixing. The RMSD between GC_2m and observed diel PM_{2.5} improves on GC_Base for most seasons and subregions (Table S1).



375

Figure 8. Seasonal and regional diel profiles of GEOS-Chem $PM_{2.5}$ from different simulation designs (Table 1). Vertical lines indicate the spatial standard deviations of seasonal mean $PM_{2.5}$ for the FEM measurements at each hour in a certain subregion.

380

Fig. 9 shows the annual-mean diel variation in $PM_{2.5}$ chemical composition for the contiguous US. The pronounced nighttime $PM_{2.5}$ peak in the base case simulation is driven primarily by nitrate and to a lesser extent by organics. Hourly emissions reduce nighttime concentrations of both species, primarily reflecting diminished nighttime emissions of NH_3 , NO_x , and organic carbon. Accounting for vertical representativeness further reduces nighttime concentrations of nitrate. The overestimation of nitrate aerosols has been a longstanding issue in GEOS-Chem (Heald et al., 2012; Zhu et al., 2013; Zhai et al., 2021). We find that development of processes to improve the diel variation of $PM_{2.5}$ also contributes to reducing the overestimation of simulated nitrate versus observations (Fig. S5).

385

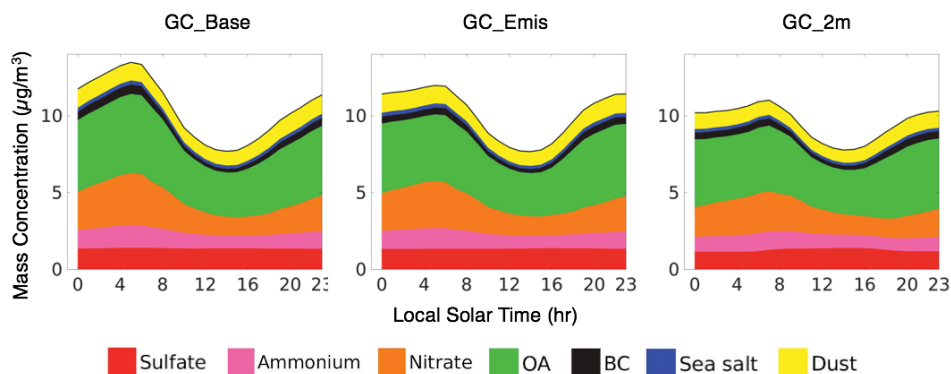
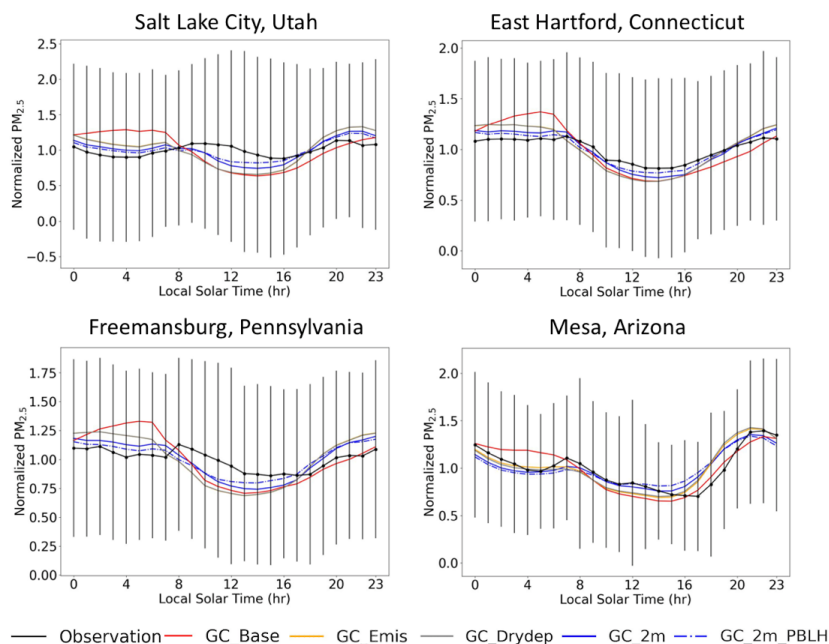


Figure 9. Annual diel profiles of $PM_{2.5}$ composition over the US in the GEOS-Chem simulations (Table 1).

Overall, we find that the driving forces of the typical diel $PM_{2.5}$ mass variation over the US reflects a complex interplay of PBL dynamics, emissions and photochemistry. The initial concentration peak in mid-morning occurs as combustion activities are emitted into a shallow mixed layer. Subsequent ventilation by vertical mixing dominates as the boundary layer develops, leading to a decrease of $PM_{2.5}$ until late afternoon despite enhanced photochemical production. The subsequent collapse at the mixed layer during sunset confines $PM_{2.5}$ emissions to the surface layer with a relative higher but diminishing concentration throughout the night as low nocturnal emissions foster a concentration minimum or flatness between midnight and early morning (Fig. 8). To further reveal the underlying driving forces, we focus on several example sites on which GC_2m well reproduces the observed overnight $PM_{2.5}$ variation. Fig. 10 shows four example sites where the $PM_{2.5}$ concentrations overnight in the GC_Base simulation are substantially overestimated. By accounting for the hourly variation in anthropogenic emissions, in GC_Emis, the simulation starts to successfully reproduce the $PM_{2.5}$ decrease or flatness overnight. By further correcting for the vertical representativeness differences, in GC_2m, the simulation more closely represents the FEM measurements. These sensitivity simulations reinforce that the internal driving forces of the $PM_{2.5}$ minimum or flatness from midnight to early morning reflects a combination of the decrease of anthropogenic emissions by weaker anthropogenic activities, while resolving the vertical representativeness differences between model and observations.



405 **Figure 10. Diel $PM_{2.5}$ mass variation in the GEOS-Chem simulations (Table 1) and the in situ measurements over four example FEM sites.**

Despite the pronounced improvement in simulating the $PM_{2.5}$ diel variation, positive biases remain in early morning in most regions and seasons (Fig. 8). The regional and seasonal variation in $PM_{2.5}$ chemical composition offers insight (Fig. S6). Nitrate appears to be an important contributor to the bias, likely reflecting insufficient vertical and horizontal resolution in our simulations to fully resolve nocturnal stratification and horizontal source separation (Zakoura and Pandis, 2018; Boys 2022). The remaining evening bias in the Spring, Summer, and Winter in the central US could reflect the possible underestimation of residential emissions in NEI (Trojanowski et al., 2022). Fig. S3 shows that the OC emissions as a relevant indicator of residential combustion are the weakest in the evenings for spring, summer, winter in Central US.

In summary, emissions, vertical representativeness differences between model and observations, boundary layer mixing, are found to be the top three contributing factors of the diel biases in GEOS-Chem $PM_{2.5}$. Dry deposition and scavenging by the formation of dew are relatively unimportant. The vertical correction for the representativeness differences by using the resistance-in-series method is critical for improving the simulation of the $PM_{2.5}$ diel amplitude as well as capturing the timings of the observed $PM_{2.5}$ morning peak and afternoon minimum, indicating the significance of vertical resolution of GEOS-Chem for simulating diel $PM_{2.5}$. Reducing the daytime positive biases in GEOS-FP PBLH and improvements of the diel representation of residential combustion may be useful to further improve the diel $PM_{2.5}$ in GEOS-Chem. In addition to the above impacting factors, we emphasize the necessity of running the simulation at fine spatial resolution to resolve processes affecting diel variation of $PM_{2.5}$ concentrations.



425 Comparison of the GC_2m (Table 1) simulations at $0.25^\circ \times 0.3125^\circ$ and $2^\circ \times 2.5^\circ$ against the FEM observations (Fig. S7) reveals that higher spatial resolution better enables the model to reproduce the $PM_{2.5}$ diel amplitude and the timings of the $PM_{2.5}$ morning peak and afternoon minimum. At coarse spatial resolution, the observed variations are poorly represented in the simulation even if all model updates are applied. The recent advances to the High-Performance implementation of the GEOS-Chem model (GCHP) Model with stretched grid capabilities (Bindle et al., 2021; Martin et al., 2022) enables higher spatial resolution than $0.25^\circ \times 0.3125^\circ$, which could offer improved representation of resolution-dependent processes in future analyses.

430 7 Conclusions

In this work, we used the GEOS-Chem model in its nested configuration to interpret the observed diel variation in $PM_{2.5}$ concentration for the contiguous United States. We first identified and addressed several biases of the base GEOS-Chem simulation of the diel variation of $PM_{2.5}$ mass concentrations. 1) The simulated $PM_{2.5}$ accumulation overnight was excessive in the base simulation, which disagreed with the observed concentration decrease or flatness from midnight to early morning, leading to a significantly overestimated $PM_{2.5}$ diel amplitude in the model. Second, the simulated timings of the $PM_{2.5}$ morning peak and afternoon minima were notably earlier relative to the in situ observations, especially for the morning peak (3 hours earlier).

To reveal the contributing factors to the diel $PM_{2.5}$ biases in the base simulation, we conduct sensitivity simulations in which we 1) increased the temporal resolution of anthropogenic emissions from monthly to hourly, 2) updated the dry deposition scheme, 3) resolved the vertical representativeness differences between the model and the observations, 4) corrected for the diel biases in the boundary layer heights of the model and 5) explored the impacts from dew formation.

We found that several developments aided representation of the $PM_{2.5}$ diel variation in the GEOS-Chem model. Hourly representation of emissions decreased normalized $PM_{2.5}$ concentrations at night with increases during the day. Accounting for vertical representativeness differences between the GEOS-Chem surface layer of 120m and the measurement height of 2m further decreases $PM_{2.5}$ at night, leading to better representation of the timing of the morning peak (~7am) and afternoon minimum. Developments to the dry deposition scheme aided mechanistic representation of gravitational settling and its hygroscopic dependence, albeit with negligible effects on $PM_{2.5}$ diel variation. Reduction of simulated PBLH to represent aircraft observations also aids agreement with observed $PM_{2.5}$ diel variation. These improvements also partially addressed a longstanding issue of a positive bias in simulated nitrate concentrations. Overall, the diel variation in $PM_{2.5}$ is attributed to 1) growth in $PM_{2.5}$ concentrations from midnight to mid-morning driven by increasing emissions into a shallow mixed layer, 2) subsequent decline in $PM_{2.5}$ concentrations from mid-morning to late afternoon during growth of the mixed layer, 3) rapid increase in $PM_{2.5}$ from late afternoon to evening as emissions persist into a collapsing mixed layer, and 4) subsequent weak decline in $PM_{2.5}$ concentrations as emissions diminish overnight. Despite the advances in representing and understanding $PM_{2.5}$ diel variation, minor biases remain. The importance of vertical resolution in representing $PM_{2.5}$ diel variation identifies an advantage to be offered by a forthcoming GEOS-FP dataset with increased resolution in the PBL. Recent advances in the horizontal



resolution of GEOS-Chem (Bindle et al., 2021; Martin et al., 2022) should also enable simulations with finer spatial resolution to further improve the diel performances.

460

465

470

475

480

485

490



495 *Code/Data availability.* The hourly FEM and 24-hour average FRM PM_{2.5} in situ measurements are available at https://aqs.epa.gov/aqsweb/airdata/download_files.html. The hourly RH measurements at four example sites in Fig. 6 are available at <https://www.ncei.noaa.gov/maps/lcd/>. The AMDAR PBLH data is available at <https://zenodo.org/record/3934378#.YiExLZZOk2y>.

500 *Author contributions.* YL and RVM designed the study. YL performed the model simulations and the data analysis. CL and AVD contributed to the diel analysis of PM_{2.5}. BLB contributed to the model developments of aerosol dry deposition and the correction on PM_{2.5} vertical representativeness. JM contributed to preparing emission data for the simulations. JRP contributed to the investigation on the impacts of PBLH on diel PM_{2.5}.

Competing interests. None of the authors has any competing interests.

Financial support. This work was supported by NASA Grants 80NSSC21K0508 and 80NSSC21K0429.

505 *Acknowledgements.* Thanks Ethan W. Emerson and Delphine K. Farmer for constructive comments about the science of aerosol dry deposition.

510

515

520

525



530 **References**

- Beckett, K. P., Freer-Smith, P. H., & Taylor, G. (1998). Urban woodlands: their role in reducing the effects of particulate pollution. *Environmental pollution*, 99(3), 347-360.
- Bessagnet, B., Pirovano, G., Mircea, M., Cuvelier, C., Aulinger, A., Calori, G., ... & Thunis, P. (2016). Presentation of the EURODELTA III intercomparison exercise-evaluation of the chemistry transport models' performance on criteria pollutants and joint analysis with meteorology. *Atmospheric Chemistry and Physics*, 16(19), 12667-12667.
- 535
- Bey, I., Jacob, D. J., Yantosca, R. M., Logan, J. A., Field, B. D., Fiore, A. M., ... & Schultz, M. G. (2001). Global modeling of tropospheric chemistry with assimilated meteorology: Model description and evaluation. *Journal of Geophysical Research: Atmospheres*, 106(D19), 23073-23095.
- 540
- Bindle, L., Martin, R. V., Cooper, M. J., Lundgren, E. W., Eastham, S. D., Auer, B. M., ... & Jacob, D. J. (2021). Grid-stretching capability for the GEOS-Chem 13.0.0 atmospheric chemistry model. *Geoscientific Model Development*, 14(10), 5977-5997.
- Boys, B. (2022). *Global Trends in Satellite-derived Fine Particulate Matter & Developments to Reactive Nitrogen in a Global Chemical Transport Model [Doctoral dissertation]*.
- 545
- Businger, J. A., Wyngaard, J. C., Izumi, Y., & Bradley, E. F. (1971). Flux-profile relationships in the atmospheric surface layer. *Journal of the atmospheric Sciences*, 28(2), 181-189.
- Du, Q., Zhao, C., Zhang, M., Dong, X., Chen, Y., Liu, Z., ... & Miao, S. (2020). Modeling diurnal variation of surface PM_{2.5} concentrations over East China with WRF-Chem: impacts from boundary-layer mixing and anthropogenic emission. *Atmospheric Chemistry and Physics*, 20(5), 2839-2863.
- 550
- Emerson, E. W., Hodshire, A. L., DeBolt, H. M., Bilsback, K. R., Pierce, J. R., McMeeking, G. R., & Farmer, D. K. (2020). Revisiting particle dry deposition and its role in radiative effect estimates. *Proceedings of the National Academy of Sciences*, 117(42), 26076-26082.
- Fairlie, T. D., Jacob, D. J., & Park, R. J. (2007). The impact of transpacific transport of mineral dust in the United States. *Atmospheric Environment*, 41(6), 1251-1266.
- 555
- Fountoukis, C., & Nenes, A. (2007). ISORROPIA II: a computationally efficient thermodynamic equilibrium model for K⁺-Ca²⁺-Mg²⁺-NH₄⁺-Na⁺-SO₄²⁻-NO₃⁻-Cl⁻-H₂O aerosols. *Atmospheric Chemistry and Physics*, 7(17), 4639-4659.
- Franchin, A., Fibiger, D. L., Goldberger, L., McDuffie, E. E., Moravek, A., Womack, C. C., ... & Middlebrook, A. M. (2018). Airborne and ground-based observations of ammonium-nitrate-dominated aerosols in a shallow boundary layer during intense winter pollution episodes in northern Utah. *Atmospheric Chemistry and Physics*, 18(23), 17259-17276.
- 560



- GBD 2019 Risk Factor Collaborators (2020). Global burden of 87 risk factors in 204 countries and territories, 1990–2019: a systematic analysis for the Global Burden of Disease Study 2019. *The Lancet*, 396(10258), 1223-1249.
- 565 Giglio, L., Randerson, J. T., & Van Der Werf, G. R. (2013). Analysis of daily, monthly, and annual burned area using the fourth-generation global fire emissions database (GFED4). *Journal of Geophysical Research: Biogeosciences*, 118(1), 317-328.
- Grell, G. A., Peckham, S. E., Schmitz, R., McKeen, S. A., Frost, G., Skamarock, W. C., & Eder, B. (2005). Fully coupled “online” chemistry within the WRF model. *Atmospheric Environment*, 39(37), 6957-6975.
- 570 Guo, J., Miao, Y., Zhang, Y., Liu, H., Li, Z., Zhang, W., ... & Zhai, P. (2016). The climatology of planetary boundary layer height in China derived from radiosonde and reanalysis data. *Atmospheric Chemistry and Physics*, 16(20), 13309-13319.
- Hammer, M. S., Martin, R. V., van Donkelaar, A., Buchard, V., Torres, O., Ridley, D. A., & Spurr, R. J. (2016). Interpreting the ultraviolet aerosol index observed with the OMI satellite instrument to understand absorption by organic aerosols: implications for atmospheric oxidation and direct radiative effects. *Atmospheric Chemistry and Physics*, 16(4), 2507-2523.
- 575 Heald, C. L., Collett Jr, J. L., Lee, T., Benedict, K. B., Schwandner, F. M., Li, Y., ... & Pye, H. O. T. (2012). Atmospheric ammonia and particulate inorganic nitrogen over the United States. *Atmospheric Chemistry and Physics*, 12(21), 10295-10312.
- Holt, J., Selin, N. E., & Solomon, S. (2015). Changes in inorganic fine particulate matter sensitivities to precursors due to large-scale US emissions reductions. *Environmental Science & Technology*, 49(8), 4834-4841.
- 580 Jaeglé, L., Quinn, P. K., Bates, T. S., Alexander, B., & Lin, J. T. (2011). Global distribution of sea salt aerosols: new constraints from in situ and remote sensing observations. *Atmospheric Chemistry and Physics*, 11(7), 3137.
- Kodros, J. K., Wiedinmyer, C., Ford, B., Cucinotta, R., Gan, R., Magzamen, S., & Pierce, J. R. (2016). Global burden of mortalities due to chronic exposure to ambient PM_{2.5} from open combustion of domestic waste. *Environmental Research Letters*, 11(12), 124022.
- 585 Li, C., Martin, R. V., Boys, B. L., van Donkelaar, A., & Ruzzante, S. (2016). Evaluation and application of multi-decadal visibility data for trend analysis of atmospheric haze. *Atmospheric Chemistry and Physics*, 16(4), 2435.
- Li, C., & Martin, R. V. (2018). Decadal changes in seasonal variation of atmospheric haze over the eastern United States: connections with anthropogenic emissions and implications for aerosol composition. *Environmental Science & Technology Letters*, 5(7), 413-418.
- 590 Lin, J. T., & McElroy, M. B. (2010). Impacts of boundary layer mixing on pollutant vertical profiles in the lower troposphere: Implications to satellite remote sensing. *Atmospheric Environment*, 44(14), 1726-1739.



- 595 Lang, J., Cheng, S., Li, J., Chen, D., Zhou, Y., Wei, X., ... & Wang, H. (2012). A monitoring and modeling study to investigate regional transport and characteristics of PM_{2.5} pollution. *Aerosol and Air Quality Research*, 13(3), 943-956.
- Malm, W. C., Sisler, J. F., Huffman, D., Eldred, R. A., & Cahill, T. A. (1994). Spatial and seasonal trends in particle concentration and optical extinction in the United States. *Journal of Geophysical Research: Atmospheres*, 99(D1), 1347-1370.
- 600 Meng, J., Martin, R. V., Ginoux, P., Hammer, M., Sulprizio, M. P., Ridley, D. A., & van Donkelaar, A. (2021). Grid-independent high-resolution dust emissions (v1. 0) for chemical transport models: application to GEOS-Chem (12.5.0). *Geoscientific Model Development*, 14(7), 4249-4260.
- Millet, D. B., Baasandorj, M., Farmer, D. K., Thornton, J. A., Baumann, K., Brophy, P., ... & Xu, J. (2015). A large and ubiquitous source of atmospheric formic acid. *Atmospheric Chemistry and Physics*, 15(11), 6283-6304.
- 605 Muskała, P., Sobik, M., Błaś, M., Polkowska, Ż., & Bokwa, A. (2015). Pollutant deposition via dew in urban and rural environment, Cracow, Poland. *Atmospheric Research*, 151, 110-119.
- Manning, M. I., Martin, R. V., Hasenkopf, C., Flasher, J., & Li, C. (2018). Diurnal patterns in global fine particulate matter concentration. *Environmental Science & Technology Letters*, 5(11), 687-691.
- Marais, E. A., Jacob, D. J., Jimenez, J. L., Campuzano-Jost, P., Day, D. A., Hu, W., ... & McNeill, V. F. (2016). Aqueous-phase mechanism for secondary organic aerosol formation from isoprene: application to the southeast 610 United States and co-benefit of SO₂ emission controls. *Atmospheric Chemistry and Physics*, 16(3), 1603-1618.
- Martin, R. V., Eastham, S. D., Bindle, L., Lundgren, E. W., Clune, T. L., Keller, C. A., ... & Jacob, D. J. (2022). Improved advection, resolution, performance, and community access in the new generation (version 13) of the high-performance GEOS-Chem global atmospheric chemistry model (GCHP). *Geoscientific Model Development*, 15(23), 8731-8748.
- 615 McDuffie, E. E., Martin, R. V., Spadaro, J. V., Burnett, R., Smith, S. J., O'Rourke, P., ... & Brauer, M. (2021). Source sector and fuel contributions to ambient PM_{2.5} and attributable mortality across multiple spatial scales. *Nature communications*, 12(1), 1-12.
- Meng, J., Martin, R. V., Li, C., van Donkelaar, A., Tzompa-Sosa, Z. A., Yue, X., ... & Burnett, R. T. (2019). Source contributions to ambient fine particulate matter for Canada. *Environmental science & technology*, 53(17), 620 10269-10278.
- Pai, S. J., Heald, C. L., Pierce, J. R., Farina, S. C., Marais, E. A., Jimenez, J. L., ... & Vu, K. (2020). An evaluation of global organic aerosol schemes using airborne observations. *Atmospheric Chemistry and Physics*, 20(5), 2637-2665.
- 625 Pai, S. J., Heald, C. L., Coe, H., Brooks, J., Shephard, M. W., Dammers, E., ... & Tibrewal, K. (2022). Compositional Constraints are Vital for Atmospheric PM_{2.5} Source Attribution over India. *ACS earth and space chemistry*, 6(10), 2432-2445.



- Park, R. J., Jacob, D. J., Field, B. D., Yantosca, R. M., & Chin, M. (2004). Natural and transboundary pollution influences on sulfate-nitrate-ammonium aerosols in the United States: Implications for policy. *Journal of Geophysical Research: Atmospheres*, 109(D15).
- 630 Polkowska, Ż., Błaś, M., Klimaszewska, K., Sobik, M., Małek, S., & Namieśnik, J. (2008). Chemical characterization of dew water collected in different geographic regions of Poland. *Sensors*, 8(6), 4006-4032.
- Pörtner, H. O., Roberts, D. C., Adams, H., Adler, C., Aldunce, P., Ali, E., ... & Fischlin, A. (2022). *Climate change 2022: Impacts, adaptation and vulnerability. IPCC Sixth Assessment Report.*
- 635 Prabhakar, G., Parworth, C. L., Zhang, X., Kim, H., Young, D. E., Beyersdorf, A. J., ... & Cappa, C. D. (2017). Observational assessment of the role of nocturnal residual-layer chemistry in determining daytime surface particulate nitrate concentrations. *Atmospheric chemistry and physics*, 17(23), 14747-14770.
- Pye, H. O. T., Chan, A. W. H., Barkley, M. P., & Seinfeld, J. H. (2010). Global modeling of organic aerosol: the importance of reactive nitrogen (NO_x and NO₃). *Atmospheric Chemistry and Physics*, 10(22), 11261-11276.
- 640 Rattigan, O. V., Felton, H. D., Bae, M. S., Schwab, J. J., & Demerjian, K. L. (2010). Multi-year hourly PM_{2.5} carbon measurements in New York: Diurnal, day of week and seasonal patterns. *Atmospheric environment*, 44(16), 2043-2053.
- Sievering, H., Enders, G., Kins, L., Kramm, G., Ruoss, K., Roeder, G., ... & Dlugi, R. (1994). Nitric acid, particulate nitrate and ammonium profiles at the Bayerischer Wald: evidence for large deposition rates of total nitrate. *Atmospheric Environment*, 28(2), 311-315.
- 645 Solomon, P. A., Crumpler, D., Flanagan, J. B., Jayanty, R. K. M., Rickman, E. E., & McDade, C. E. (2014). US national PM_{2.5} chemical speciation monitoring networks—CSN and IMPROVE: description of networks. *Journal of the Air & Waste Management Association*, 64(12), 1410-1438.
- Song, S., Ma, T., Zhang, Y., Shen, L., Liu, P., Li, K., ... & McElroy, M. B. (2021). Global modeling of heterogeneous hydroxymethanesulfonate chemistry. *Atmospheric Chemistry and Physics*, 21(1), 457-481.
- 650 Tessum, C. W., Hill, J. D., & Marshall, J. D. (2015). Twelve-month, 12km resolution North American WRF-Chem v3.4 air quality simulation: performance evaluation. *Geoscientific Model Development*, 8(4).
- Tiwari, S., Srivastava, A. K., Bisht, D. S., Parmita, P., Srivastava, M. K., & Attri, S. D. (2013). Diurnal and seasonal variations of black carbon and PM_{2.5} over New Delhi, India: Influence of meteorology. *Atmospheric Research*, 125, 50-62.
- 655 Trojanowski, R., Lindberg, J., Butcher, T., & Fthenakis, V. (2022). Realistic operation of two residential cordwood-fired outdoor hydronic heater appliances—Part 1: Particulate and gaseous emissions. *Journal of the Air & Waste Management Association*, 72(7), 738-761.



- 660 Travis, K. R., & Jacob, D. J. (2019). Systematic bias in evaluating chemical transport models with maximum daily 8h average (MDA8) surface ozone for air quality applications: a case study with GEOS-Chem v9.02. *Geoscientific Model Development*, 12(8), 3641-3648.
- van Donkelaar, A., Martin, R. V., Brauer, M., Kahn, R., Levy, R., Verduzco, C., & Villeneuve, P. J. (2010). Global estimates of ambient fine particulate matter concentrations from satellite-based aerosol optical depth: development and application. *Environmental health perspectives*, 118(6), 847-855.
- 665 van Donkelaar, A., Martin, R. V., Brauer, M., Kahn, R., Levy, R., Verduzco, C., & Villeneuve, P. J. (2021). Global estimates of ambient fine particulate matter concentrations from satellite-based aerosol optical depth: development and application. *Environmental health perspectives*, 118(6), 847-855.
- Wang, Q., Jacob, D. J., Spackman, J. R., Perring, A. E., Schwarz, J. P., Moteki, N., ... & Barrett, S. R. (2014). Global budget and radiative forcing of black carbon aerosol: Constraints from pole-to-pole (HIPPO) observations across the Pacific. *Journal of Geophysical Research: Atmospheres*, 119(1), 195-206.
- 670 Xu, J. W., Lin, J., Tong, D., & Chen, L. (2023). The underappreciated role of transboundary pollution in future air quality and health improvements in China. *Atmospheric Chemistry and Physics Discussions*, 1-25.
- Zakoura, M., & Pandis, S. N. (2018). Overprediction of aerosol nitrate by chemical transport models: The role of grid resolution. *Atmospheric Environment*, 187, 390-400.
- 675 Zhai, S., Jacob, D. J., Brewer, J. F., Li, K., Moch, J. M., Kim, J., ... & Liao, H. (2021). Relating geostationary satellite measurements of aerosol optical depth (AOD) over East Asia to fine particulate matter (PM_{2.5}): insights from the KORUS-AQ aircraft campaign and GEOS-Chem model simulations. *Atmospheric Chemistry and Physics*, 21(22), 16775-16791.
- Zhang, H., Cheng, S., Yao, S., Wang, X., & Zhang, J. (2019). Multiple perspectives for modeling regional PM_{2.5} transport across cities in the Beijing–Tianjin–Hebei region during haze episodes. *Atmospheric Environment*, 212, 22-35.
- 680 Zhang, L., Jacob, D. J., Knipping, E. M., Kumar, N., Munger, J. W., Carouge, C. C., ... & Chen, D. (2012). Nitrogen deposition to the United States: distribution, sources, and processes. *Atmospheric Chemistry and Physics*, 12(10), 4539-4554.
- 685 Zhang, L., Chen, Y., Zhao, Y., Henze, D. K., Zhu, L., Song, Y., ... & Huang, B. (2018). Agricultural ammonia emissions in China: reconciling bottom-up and top-down estimates. *Atmospheric Chemistry and Physics*, 18(1), 339-355.
- Zhang, Y., Sun, K., Gao, Z., Pan, Z., Shook, M. A., & Li, D. (2020). Diurnal climatology of planetary boundary layer height over the contiguous United States derived from AMDAR and reanalysis data. *Journal of Geophysical Research: Atmospheres*, 125(20), e2020JD032803.
- 690 Zhao, X., Zhang, X., Xu, X., Xu, J., Meng, W., & Pu, W. (2009). Seasonal and diurnal variations of ambient PM_{2.5} concentration in urban and rural environments in Beijing. *Atmospheric Environment*, 43(18), 2893-2900.



- Zheng, B., Zhang, Q., Zhang, Y., He, K. B., Wang, K., Zheng, G. J., ... & Kimoto, T.: (2015). Heterogeneous chemistry: a mechanism missing in current models to explain secondary inorganic aerosol formation during the January 2013 haze episode in North China, *Atmos. Chem. Phys.*, 15, 2031–2049.
- 695 Zhu, L., Henze, D. K., Cady-Pereira, K. E., Shephard, M. W., Luo, M., Pinder, R. W., ... & Jeong, G. R. (2013). Constraining US ammonia emissions using TES remote sensing observations and the GEOS-Chem adjoint model. *Journal of Geophysical Research: Atmospheres*, 118(8), 3355-3368.
- Zhu, L., Jacob, D. J., Kim, P. S., Fisher, J. A., Yu, K., Travis, K. R., ... & Wolfe, G. M. (2016). Observing atmospheric formaldehyde (HCHO) from space: validation and intercomparison of six retrievals from four satellites (OMI, GOME2A, GOME2B, OMPS) with SEAC⁴RS aircraft observations over the southeast US. *Atmospheric Chemistry and Physics*, 16 (21), 13477-13490.
- 700